Mode-field diameter of single-mode optical fiber by far-field scanning

Matt Young

I use the direct far-field method to measure the mode-field diameter of a single-mode fiber with an expanded uncertainty of 30 nm, with a coverage factor of 2. For a step-index fiber with a mode-field diameter of approximately 9 μm, the major sources of uncertainty are nonlinearity in the electronics, angular errors and scattered light in the apparatus, and the polarization and noncircularity of the mode of the fiber. The paper concludes by showing an inconsistency in the derivation of the far-field expression for mode-field diameter.

OCIS codes: 060.0060, 060.2270, 060.2300, 060.2430, 050.1960, 120.3940, 120.4800.

1. Introduction

The measurements and analyses that have led to an artifact standard for the mode-field diameter of a single-mode optical fiber are described. This standard is the seventh so far developed by the Fiber and Integrated Optics Group of the Optoelectronics Division of the National Institute of Standards and Technology (NIST).

The Telecommunications Industry Association (TIA) has defined the direct far-field method of measuring mode-field diameter as the "reference method, used to resolve disputes."[1] The far-field method is thus considered definitive, and other methods must agree with the far-field method if they are to be considered valid measurements. The direct far-field method consists of a far-field scan; that is, a detector that is linear in optical power is scanned in an arc at whose center lies the exit face of the fiber specimen.

The TIA method specifies a detector that is linear over at least 4 orders of magnitude (40 dB). If 0 is the center of the far-field radiation pattern, then the detector must scan an arc that is typically from −21° to +21° in steps no greater than 0.5°, and the pinhole in front of the detector must subtend an angle no larger than 0.5°. The measurement must also include a cladding-mode stripper, which is often simply the polymer coating, and a 3-cm-diameter loop of fiber to remove higher-order modes if necessary.

The author is with the Optoelectronics Division, National Institute of Standards and Technology, 325 Broadway, Boulder, Colorado 80303.

Received 9 February 1998; revised manuscript received 8 May 1998.

The criteria concerning the angular step and the pinhole diameter are almost always adequate. The range of ±21°, however, is inadequate for certain types of fiber. A better criterion would state, for example, that the measurement must be continued until the detector photocurrent falls to a specified fraction of its maximum value and remains below that specified fraction. That fraction may be more than 4 orders of magnitude below the maximum intensity.

The mode-field diameter is calculated from a relation first derived by Petermann and elaborated by Pask.[2] Artiglia and co-workers[3] derived from Pask's formulation the equation that is used today in the TIA standard:

$$2w_0 = (\lambda/\pi)\left[2\int I(\theta)\sin\theta\cos\theta\,d\theta\Big/\int I(\theta)\sin^3\theta\cos\theta\,d\theta\right]^{1/2}, \quad (1)$$

where $2w_0$ is the mode-field diameter, λ is the mean wavelength of the light, θ is the angle with respect to the center of the radiation pattern, and the integrations are carried out, in principle, from 0° to 90°. The standard implicitly considers Eq. (1) and Petermann's relation to be equivalent. I note several problems with Eq. (1) below. Specifically, Pask's formulation assumes implicitly that the amplitude distribution, or pattern, in the exit face of the fiber has radial symmetry. More fundamentally, Eq. (1) is a nonparaxial formulation, but its derivation improperly ignores the obliquity factor; a formulation that

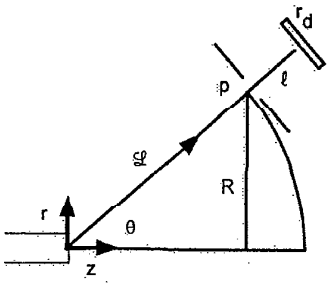

Fig. 1. Schematic drawing of the far-field scanner showing the fiber, pinhole, and detector.

retains the obliquity factor results in integrals that do not converge. Finally, Petermann's relation uses the mode of the fiber, whereas the field at the end of a truncated fiber differs from the mode. For practical reasons, I therefore suggest that Eq. (1), not Petermann's relation, be adopted as the definition of mode-field diameter. Petermann's relation and Eq. (1) are not equivalent.

In this paper I describe the far-field scanner set up at NIST to certify mode-field diameter standards, and I estimate the standard uncertainty of the measurements performed on this apparatus. The scanner was designed to provide linearity over 6 orders of magnitude and can scan an arc from +40° to −40° if necessary. In addition, scattered light has been minimized because a constant scattered power added to the measurement can bring about a significant systematic error.

2. Apparatus

The apparatus is shown in Fig. 1. It consists of a rotation stage under computer control and is the same stage that we used earlier for measurements on multimode fibers.[4] I improved the system by adding a lock-in amplifier and a mechanical chopper, as well as by constructing a black backdrop (not shown) and painting most of the apparatus with a proprietary flat black paint. I used two sources, both Fabry–Perot lasers, with wavelengths around 1310 and 1550 nm. In addition, I replaced the old Ge detector with an InGaAs photodiode for use at these wavelengths.

A typical single-mode fiber has a mode-field radius w_0 around 5 μm. The TIA requires the distance between the exit face of the fiber and the detector to be at least $100 \times w_0^2/\lambda$, where w_0^2/λ is the distance at which a circle of radius w_0 occupies one Fresnel zone.[5] w_0^2/λ is an arbitrary dividing line between the near field and the far field, but the measured intensity close to this dividing line does not closely approximate the calculated far-field pattern. For better agreement with theory, the distance between the fiber and the detector has to exceed at least 10 times w_0^2/λ, depending on the accuracy required. The TIA criterion is 100 times, or approximately 2 mm. In our system, we use approximately 130 mm. I therefore assume that no measurable error can arise from the fact that this distance is finite.

The rotation stage drives the detector in a horizontal arc. It uses a stepping motor whose steps correspond to angular increments of (1/240)°. The computer takes measurements every 96 steps, or 0.4°, which I call a giant step. Previous experience with this stage showed that it rotated through a complete circle, or 86,400 steps, with an imprecision well under 1 step. Errors that result from machining tolerances, however, amount to approximately 3 arc min or 0.05°, that is, 12 steps. The major source of these errors is a periodic error in the shaft of the motor.

The lasers are Fabry–Perot lasers with linewidths of around 2 nm. They are mounted in fixtures that control their temperatures within 0.1 °C, and their input currents of 40 or 50 mA are controlled within 0.1 mA. The lasers are pigtailed directly to single-mode fibers, so the radiation is brought briefly into air and collimated to accommodate a mechanical chopper, which is needed for phase-sensitive detection. The beam is then refocused into a second single-mode fiber. One end of the specimen is connected to this fiber by means of a commercial splice that contains an oil-filled capillary. All the fibers are constrained so that they cannot move, especially during polarization-sensitive measurements, either with pressure-sensitive tape or a weighted layer of foam rubber.

The other end of the specimen is cleaved perpendicularly to its axis with a commercial cleaver and located at the center of rotation of the stage by means of a microscope and a cross hair. This is a critical step: *An error in the position of the fiber will result* in an error of the measurement. To locate the cross hair along the axis of rotation of the stage, I had a brass pin machined to fit tightly into a hole at the center of the stage. The pin comes to a point near the desired location of the fiber end. The point comes within 100 μm of the axis of the stage. However, by rotating the stage or (what turns out to be equivalent) the pin, I can easily locate the cross hair within 25 μm of the axis.

After locating the fiber end along the axis of rotation, I revolved the detector about that axis until the photocurrent is a maximum; this ensures that the *detector is located along the axis of the fiber and* needs to be done only once. Thereafter, I located the fiber end with the cross hair and then adjusted it laterally and vertically but not axially with a three-axis translation stage until the photocurrent is a maximum. The lateral and vertical adjustments are necessary because the end of the fiber is not precisely perpendicular to the axis.

The detector is a 2-mm InGaAs photodiode at the end of a 130-mm arm and always points toward the fiber end. Its housing also accommodates a 0.5-mm pinhole, which I deliberately located about 1 cm from the detector so as to limit the field of view of the detector and thereby discriminate against stray light. The output of the photodiode goes into the low-impedance input of a lock-in amplifier. The detector

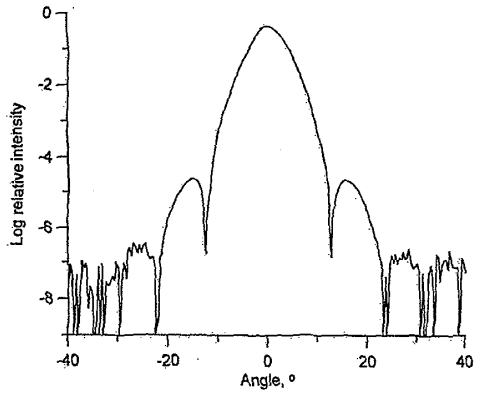

Fig. 2. Far-field scan of a step-index fiber at 1310 nm. The logarithm of intensity is plotted as a function of angle.

had to be electrically isolated from the rotation stage to eliminate what were apparently ground loops.

The lock-in amplifier has a small zero offset, which I corrected on each scale by issuing an offset command. I checked between-scale linearity by measuring a given power on two adjacent scales. The scale factors varied by as much as 4% of their nominal values, although the important scales, where the photocurrent is highest, differed from one another by only a few tenths of 1%. I corrected this defect with software and saved the corrected data.

I checked for saturation by inserting a filter directly in front of the pinhole and measuring the transmittance of that filter at each scale on the lock-in amplifier. I used a colored glass filter, rather than a metal-coated filter, to reduce the possibility of multiple reflections within the glass. To reach every scale on the lock-in amplifier, I controlled the power by revolving the detector about the fiber end until it reached the intensity that brought about a nearly full-scale reading on each scale. The filter had to be perpendicular to the incoming pencil of rays to avoid deflecting that pencil; if the pencil were deflected, the pinhole would sample a different part of the wave front than when the filter was absent. Because the filter had to be removed and replaced repeatedly, I built a small fixture to ensure that the filter would always be inserted in the same place and in the same orientation. All scales gave substantially the same transmittance, generally within a fraction of 1%, so correction for saturation was not necessary. I did not check whether the gain of each scale was a constant but rather treated within-scale nonlinearity as an uncertainty.

Figure 2 shows a scan of a step-index fiber whose mode-field diameter is approximately 9 μm. The cusps at approximately ±13° are zero crossings of the electric field; that the intensity at those zero crossings does not go much below 10^{-6} is a measure of the scattered light in the system. Beyond approximately 40°, the detector responds to scattered light whose relative intensity is no more than 3×10^{-7}, but sidelobe power is sometimes barely visible at those angles when the cleave of the fiber is exceptionally good. Figure 2 is an exceptionally good scan that shows the second and third sidelobes well.

A liberal application of the proprietary flat black paint was needed to reduce the scattered intensity below 10^{-6}. This paint covers the detector arm, the backdrop, and the mechanism that holds the fiber. To ascertain the source of the remaining scattered light, I performed a radiometric analysis using the paraxial approximation and the notation and formalism of Ref. 6. Briefly, if P is the total power emitted by the fiber, then the average irradiance E of the black backdrop is $P/\pi w^2$, where w is the radius of the radiation pattern at a distance D from the fiber end and D is the distance between the fiber end and the backdrop. The corresponding radiance is $L = KE/\pi$, where K is the diffuse reflectance of the backdrop. The light scattered from the backdrop and onto the structure that holds the fiber gives rise to an irradiance $E' = KP/\pi D^2$ in the plane of the structure. The corresponding radiance of the structure in the plane of the fiber end is $L' = KE'/\pi$, where I assume that the reflectance of the structure is the same as that of the backdrop.

Because the pinhole is approximately 1 cm from the detector, the field of view of the detector is only a small area around the fiber end. This area depends on the radius r_d of the detector, its distance l from the pinhole, and the distance $\mathcal{L}$ between the fiber end and the pinhole; its radius is given by $(r_d/l)\mathcal{L}$. Using similar triangles, we find that the total power scattered from this area into a pinhole of radius p is $(Kr_d p/\mathcal{L}l)^2 P \cos\theta$, when the detector is off axis by an angle θ (see Fig. 1).

Only a fraction of the total power emitted by the fiber passes through the pinhole when the detector is located exactly at the center of the radiation pattern. If the fiber mode is a Gaussian beam, then that fraction is $2P(p/w)^2$. The ratio of the scattered power to the power that falls onto the detector when it is in the center of the radiation pattern is therefore $f = (1/2)(Kr_d w/\mathcal{L}l)^2 \cos\theta$. If $K = 0.01$ and $\theta = 40°$, then $f = 3 \times 10^{-9}$. The measured value at 40°, where the specularly transmitted light from the fiber end is small, however, is approximately 3×10^{-7}.

To assess the accuracy of the radiometric calculation, I placed a piece of diffuse white paper in the plane of the fiber. To avoid disturbing the fiber, I located the paper below the fiber end so that it covered only approximately one half of the field of view of the detector. If the diffuse reflectance of the paper is 0.9, then the ratio f becomes $3 \times 10^{-9} \times (0.9/0.01) \times (1/2) = 1.5 \times 10^{-7}$. The measured value is 4.5×10^{-7}; that is, the white paper increased the value of f by approximately 1.5×10^{-7}, which is in agreement with the calculation.

It seems, therefore, that the scattered light originates from the surface of the fiber itself. To see whether this conclusion is plausible, I estimated the value of f that would arise as a result of surface roughness on the cleaved end of the fiber. As long as

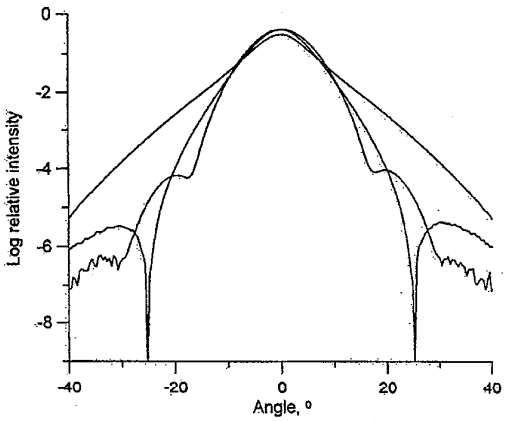

Fig. 3. Far-field scans of two step-index fibers and one dispersion-compensating fiber at 1310 nm.

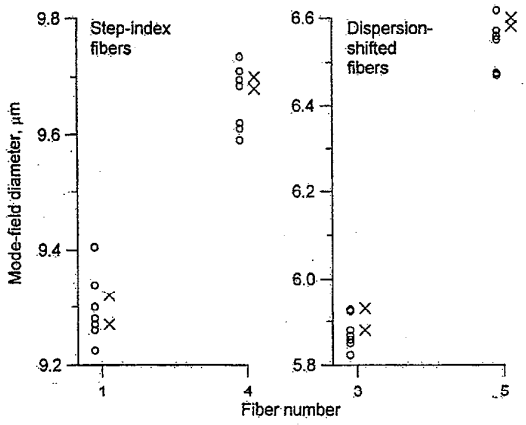

Fig. 4. Comparison of the results of this study (crosses) with an earlier interlaboratory comparison (open circles) of mode-field diameters of two step-index fibers and two dispersion-shifted fibers. Each circle represents the result of a different laboratory.

the correlation length of the surface features is longer than approximately 2λ, the total power scattered into a hemisphere by a reflector is $P/P_0 = (2k\sigma)^2R$, where P_0 is the power incident on the surface, $k = 2\pi/\lambda$, σ is the rms surface roughness, and R is reflectance.[7] For a surface in transmission, we have to replace 2 with $(n - 1)$ and R with the transmittance T of the surface. That is, for our case, $P/P_0 = [k(n - 1)\sigma]^2T$. By an analysis similar to that above, we find that the ratio $f = 2[k(n - 1)\sigma]^2T(w/\mathcal{L})^2 \cos\theta$. If $\sigma = 2$ nm, a good but not unrealistic surface finish, we obtain approximately 2.6×10^{-7}, whereas the measured value is 3×10^{-7}.

The evidence strongly suggests that the scattered light emanates from the end of the fiber. Furthermore, although most of the few step-index fibers I tested are similar, scans of two other fibers displayed either more or less scattered light. Figure 3 shows far-field scans of those two step-index fibers, as well as a dispersion-compensating fiber (not a dispersion-shifted fiber), all at 1310 nm. The cusps in the step-index fibers' patterns are zero crossings of the electric field; that they differ from 0 is a measure of the scattered intensity at those angles. One of the fibers evidently has a poor surface finish, whereas the other has a very good finish. It is not, however, possible to ascertain whether the dispersion-compensating fiber scatters significant power because its radiation pattern is wider than the 40° of the scan. Because a scattered-light ratio of 10^{-5} can affect the results (see below), this militates in favor of using a step-index fiber for a standard.

3. Results

Some typical and atypical results are shown in Figs. 2 and 3. In addition, I located four fibers that had been used in a round robin (interlaboratory comparison) of mode-field diameter measurements.[8] Two of these fibers are step-index fibers, whereas the other two are dispersion-shifted fibers. Following the TIA procedure, I cut the requisite 2.2 m of each fiber and prepared new ends. For each specimen, I measured the mode-field diameter at 1310 nm and then cut a new end and performed a second measurement. The results are displayed as the crosses in Fig. 4. The open circles in that figure are the round robin data. Each circle represents a datum submitted by a single participant. Each datum is the average of one measurement on each of two newly prepared ends.

The agreement is good, although my measurements of the dispersion-shifted fibers fall slightly on the high side of the mean of the round robin measurements. It is hard to ascribe much significance to this fact, particularly because much of the scatter in the data may be the result of variations in the fibers and we have no estimate of the measurement uncertainty of the participants. Nevertheless, no participant's data disagree with NIST data by more than a smidgen over 0.1 μm.

4. Uncertainty Analysis

I performed the uncertainty analysis on the step-index fiber of Fig. 2. Its near-field intensity is approximately Gaussian, as verified by near-field scanning. I performed most of the analyses in two ways: First I assumed a Gaussian intensity in both the near and the far fields and estimated the errors mathematically. Second, I deliberately introduced errors into the experimental setup and calculated the resulting mode-field diameter. In general, the calculations agreed well with the experiment.

A. Note on Terminology

When I say error, I mean the difference between a measured value and the (hypothetical) true value of a quantity, whether that quantity is an independent variable such as the position of the fiber end or the measurand itself. Repeated observations of the same measurand will yield different values and therefore different errors. The mean value of the set of repeated measurements is an estimator of the true

Table 1. Mode-Field Diameter Calculated for Various Angular Increments, Simulated Data

Increment (deg)	Number of Points	Angular range (deg)	Trapezoidal Rule	Extended Trapezoidal Rule	Simpson's Rule
0.4	53	21.2	9.071	9.080	9.080
0.6	35	21	9.060	9.082	9.080
0.8	26	20.8	9.045	9.085	9.081

[a]All the results are in micrometers.

value. The range of measured values is one component of the uncertainty associated with the mean value.

Many uncertainties cannot be measured but must be estimated. I state such uncertainties in terms of what is essentially a 100% confidence interval (strictly, the smallest 100% confidence interval; an extremely wide interval obviously yields 100% confidence, but it is not useful). Confidence interval is a term that is borrowed from statistics; for example, a confidence interval of 99.7% corresponds to 3 standard deviations of the mean value of a Gaussian random variable. I use the term somewhat imprecisely to describe uncertainties that cannot be obtained by statistical means and whose confidence intervals therefore must be estimated. Specifically, I estimate the largest probable error and use that estimate to define the 100% confidence interval, but I assume that the probability distribution for such errors is flat over the interval.

I combine components of uncertainty by adding the variances of the presumed probability distributions in quadrature, what is commonly called the root-sum-of-squares method, whether or not an error is identified as random or systematic.[9] This is equivalent to assuming that the components of the uncertainty are small and uncorrelated or, more precisely, that I succeeded in categorizing the components of uncertainty in such a way that they are small and uncorrelated. Here the variance of a Gaussian distribution is the square of its standard deviation, whereas the variance of a rectangular distribution is equal to the half-width of the distribution divided by 3. The square root of any variance is called the standard uncertainty and is analogous to standard deviation in statistics. The standard uncertainty of a rectangular distribution equals its half-width divided by $\sqrt{(3)}$.

Some uncertainties result from systematic errors, or biases. Then the confidence intervals are asymmetric about the true value. Specifically, the confidence interval may extend from 0 to some value $2x$. In such cases, I generally subtract the value x from the experimental result, so the confidence interval extends from $-x$ to x.

B. Numerical Integration and Angular Increment

The sampling theorem[10] can be used to estimate the largest useful angular increment, or giant step. It applies only to band-limited functions, and the near-field pattern of a fiber is only approximately band limited. Nevertheless, let us treat the near-field pattern as if it were a band-limited function whose (single-sided) bandwidth is perhaps $3w_0$. If the amplitude is an approximately Gaussian function of radius, then at the radius $3w_0$ the amplitude is a factor of $e^{-9} \sim 10^{-4}$ below its value at the center of the fiber. The sampling theorem applied to our case prescribes that the angular increment must be less than $\lambda/(2 \times 6w_0)$, where $6w_0$ is the full-width of the near-field pattern. If we take $\lambda = 1.3$ μm and $w_0 = 4.5$ μm, we find that $\lambda/(2 \times 6w_0) = 1.4°$. In fact, that angular increment would give a measurable error, presumably because the near-field pattern is not truly band limited (Table 1).

I used a simulation to determine the errors that might arise as a result of the numerical integration. There are two considerations: the range of the scan and the angular increment between measurements. Here we consider the angular increment. I assumed that the near-field pattern of the fiber was a Gaussian function with $w_0 = 9.08$ μm, in agreement with a specific fiber end I had been studying, and $\lambda = 1.308$ μm. The far-field intensity pattern that results from this near-field pattern is

$$I(\theta) = \exp(-2 \sin^2 \theta / \sin^2 \theta_0), \qquad (2)$$

where $\sin \theta_0 = \lambda/\pi w_0$ is the numerical aperture of the fiber. It is important to use $\sin \theta_0$ rather than θ_0 in all calculations; the paraxial approximation will result in a potentially significant error, as has been noted elsewhere.[11]

I used Eq. (1) with various angular increments to calculate the mode-field diameter that corresponds to Eq. (2). Specifically, I used a trapezoidal rule, an extended trapezoidal rule, and Simpson's rule[12] to numerically integrate a discrete data set derived from Eq. (2). As long as the scanning range is large enough, the rectangular rule yields the same result as the trapezoidal rule, because the first and last terms in the integrands are 0.

All three methods gave consistent results at any range that equaled or exceeded the TIA's specified value of 21°. The trapezoidal rule, however, did not yield the correct value of 9.080 μm, as shown in Table 1, but resulted in an error of 9 nm.

I used the extended trapezoidal rule, in part simply because I began with it. (Simpson's rule was more accurate at coarser scans, but the extended trapezoidal rule was adequate when the angular increment

was 0.4°.) The definite integral of a function $f(x)$ over the interval from x_1 to x_2 is given by

$$\int f(x)dx = [(3/8)f_1 + (7/16)f_2 + (23/24)f_3 + f_4 + f_5 + \cdots + f_{N-4} + f_{N-3} + (23/24)f_{N-2} + (7/6)f_{N-1} + (3/8)f_N]\delta x, \quad (3)$$

where δx is the step size and N is the number of increments. I assume that the standard uncertainty brought about by the numerical integration is less than 1 nm (0.01%), although it could be significant with a different type of fiber.

C. Angle of Scan

The scan is taken from $-\theta_m$ to θ_m, and the value of θ_m may affect the result. This is so because taking a finite scan is precisely equivalent to using a lens with a finite numerical aperture. The far-field pattern is assumed to be the Hankel transform of the near-field pattern (but see below). If we scan over a finite angular range, we clip the Hankel transform, that is, multiply it by a circ function (the terminology is that of Gaskill[13]; $\mathrm{circ}(r/a) = 1$ when $r < a$ and 0 otherwise). The resulting near-field pattern is therefore the convolution of the true near-field pattern with a sombrero function $2J_1(\beta/\beta)$, where J_1 is the first-order Bessel function, $\beta = (1.22\pi r/RL)$, $RL = 0.61\lambda/\sin\theta_m$, and r is the radial dimension in the near field. The sombrero function is identical to the impulse response of a diffraction-limited lens whose numerical aperture is $\sin\theta_m$. I therefore use the term numerical aperture to describe the scanning range. A scan with a finite numerical aperture results in a broadened near-field intensity, or a calculated mode-field diameter that is larger than the true value.

To assess the effect of numerical aperture on measured diameter, I again used Eqs. (1) and (2) with $w_0 = 9.08$ μm and an increment of 0.4°. The extended trapezoidal rule gave an error of +16 nm when $\theta_m = 10.4°$ but an error less than +1 nm when $\theta_m > 15.2°$.

It is not uncommon to assume not only that the electric-field pattern in the exit face of the fiber is Gaussian but also that the Airy disk can be approximated by a Gaussian function whose radius g is roughly equal to the resolution limit RL. Convolution of two such Gaussian functions results in the convenient rule $w^2 = w_0^2 + g^2$, where w is the radius of the resulting function. In our case, $RL = 0.61\lambda/\sin\theta_m$ and $\theta_m = 21°$, so RL = 2.2 μm. If $w_0 = 9.08$ μm, then $w = 9.35$ μm, and the error $w - w_0$ is 270 nm. This is a gross overestimate; convolving with a sinc or a sombrero function broadens a given function much less than convolving with a Gaussian function that has the same half-width or radius.

I next took two real data sets, one for a step-index fiber and one for a dispersion-compensating fiber. Each data set extended from −40° to 40°, and I calculated the mode-field diameter with values of θ_m from 15.2° to 40°. The result is shown in Table 2;

Table 2. Measured Mode-Field Diameter as a Function of Maximum Scanning Angle

Angle (deg)	Step-Index (μm)	Dispersion-Compensating Fiber (μm)
15.2	9.116	4.647
18	9.091	4.292
21.2	9.081	4.045
24	9.081	3.916
26	9.080	3.858
28	9.079	3.818
30	9.079	3.792
36	9.078	3.760
40	9.077	3.754

evidently the value of 21° is adequate for the step-index fiber but not for the dispersion-compensating fiber. Although noise may be a factor, the step-index fiber seems to converge toward 9.075 or thereabouts, or 6 nm less than the value calculated with $\theta_m = 21.2°$. The dispersion-compensating fiber also may approach an asymptote around 40° or 45°, but the value at 21.2° is in error by at least 300 nm.

I took the error introduced by truncating the measurement at 21° to be approximately +5 nm for the step-index fiber. Thus, to compensate for the systematic nature of the error, we subtract 5 nm from the measured value but, to be conservative, also assume a 100% confidence interval of 5 nm. The standard uncertainty is $5/\sqrt{3}$ nm ≈ 3 nm.

A fiber with a substantially different mode-field diameter has to be analyzed similarly. The correction of 5 nm is specific to this fiber only and will differ from 5 nm if the far-field pattern differs from the far-field pattern of this specimen or if the angle of scan differs from 21°. The dispersion-compensating fiber, for example, will require a scan to at least 40°, a fact already noted by Anderson and colleagues in their discussion of dispersion-shifted fibers.[14]

D. Angular Errors

The manufacturer specifies the angular accuracy of the stage to be ±3 arc min. The major source of the angular errors is machining tolerance in the manufacture of the motor. Therefore errors do not accumulate but rather are periodic, with a period equivalent to one rotation of the shaft, or 400 steps. We might try to estimate the effect of an angular error by noting that the half-angle of the far-field radiation pattern is approximately 5°. If we were to search for the $1/e^2$ intensity, we would encounter an angular uncertainty up to 3 arc min, or 9×10^{-4} rad. The corresponding value of w_0 will be in error by as much as (3 arc min/5°) × w_0, or 90 nm. This value is unacceptably large and shows that it is necessary to use all the data, either by a curve fit or by the TIA method, rather than to search for a single point.

To include the periodic error in the simulation, I replaced θ with $\theta + m\sin(2\pi\theta/\Pi)$, where $m = 9 \times 10^{-4}$ rad is the maximum error and $\Pi = 0.029$ rad is the period of the error and corresponds to one rotation

of the shaft. The calculated mode-field diameter is in error by 10 nm, as opposed to the 90 nm obtained by the estimate. (Integrating real data with an added periodic error gives a similar result, although this calculation is problematic in that it could have added one uncertainty to another.) Because m is the greatest expected angular error, I took 10 nm/$\sqrt{3}$ nm $\approx$ 6 nm to be the standard uncertainty that is due to angular errors.

E. Finite Pinhole

The far-field pattern recorded by the detector is the convolution of the true pattern with the circ function that represents the pinhole. According to the convolution theorem, therefore, the recorded near-field pattern is the product of the true near-field pattern and the Hankel transform of the circ function. That is, Eq. (1) calculates not the mode-field diameter of the true near-field pattern but rather the mode-field diameter of that product. Because the far-field pattern is broadened by the finite pinhole, the near-field pattern is narrowed. That is, we can expect a value that is always less than the true value of the mode-field diameter.

The Hankel transform of the pinhole is $2J_1(1.22\pi r/\rho)/(1.22\pi r/\rho)$, where r is the radial dimension in the exit face of the fiber and $\rho = 0.61\lambda L/p$. To estimate the error that results from the finite pinhole, I multiplied the Gaussian function $\exp(-2r^2/w_0^2)$ by the Hankel transform and calculated the value of ρ for which the intensity was $1/e^2$. For typical values of w_0 and λ, the resulting error in the mode-field diameter is roughly -8 nm.

Provided that the mode-field pattern of the fiber is close to a Gaussian function, then we can add 8 nm to the calculated value and thereby correct for the finite pinhole. That is, the value of 8 nm is not an uncertainty but rather a correction. Let us guess that the uncertainty of the correction is no more than 4 nm, or half the correction itself. Then the standard uncertainty is 4/$\sqrt{3}$ nm $\approx$ 2 nm.

F. Repeatability and Noise

If a fiber is placed in the setup and nothing is moved, several measurements in succession are repeatable within a few nanometers. This suggests that the effect of electronic noise is also only a few nanometers. I simulated electronic noise by adding a Gaussian random variable[15] to Eq. (2).

The short-term stability of the laser and the electronics is approximately 0.6 parts in 440. Call that value 6 standard deviations. Then 1 standard deviation is 2×10^{-4}. I modeled these fluctuations by replacing $I(\theta)$ with $I(\theta)(1 + n)$, where n represents a Gaussian random variable whose mean is 0 and whose standard deviation is 2×10^{-4}. This is equivalent to assuming that the fluctuations derive from fluctuations in the laser power, the gain or noise of the amplifier, or the rotation speed of the chopper. I calculated the mode-field diameter a number of times and calculated the sample standard deviation, which was under 1 nm. I similarly calculated the mode-field diameter for purely additive noise with a standard deviation of 10^{-6}, which is roughly the noise floor in Fig. 2. Again, the sample standard deviation was approximately 1 nm. These values are consistent with the observation that repeated measurements yield values that are within a few nanometers of each other.

Physically removing and replacing the fiber yields a repeatability of perhaps 5 nm. It seems likely, however, that at least some of the loss of repeatability is due to polarization and noncircularity and some to positioning errors, all of which are discussed below. It is important not to mistakenly include the same source of uncertainty twice, so I took repeatability to mean the repeatability of measurements taken in quick succession. Lack of repeatability in this sense is primarily the result of electronic noise, and I estimated the standard uncertainty to be 3 nm.

G. Gain Nonlinearity

I examined two cases of gain nonlinearity: between scale and within scale. The experiments described above showed that the error introduced by changing from one scale to an adjacent scale was a few tenths of 1%, except for the most sensitive scales, where the photocurrent was least. Over the first three decades of intensity or photocurrent, the error that was due to scale change accumulated to approximately 0.4%. I attempted to correct this error in the software, but with only partial success, as judged by repeated calibrations. For uncertainty analysis, therefore, I assumed that the gain of the electronics (that is, the lock-in amplifier and the detector) was a linear function of intensity and varied between 0.99 and 1 as the intensity varied between 0 and the maximum. I again assumed that the far-field intensity pattern is a Gaussian function and multiplied that function by the gain. The calculated mode-field diameter differed from the true value by 12 nm.

The manufacturer specifies that the gain of the lock-in amplifier is linear within 1%, and the measured transmittances of the filter were always within 1% of each other. These transmittances, however, were always measured on the same part of the scale, so these filter experiments tell nothing about within-scale linearity. I assumed, therefore, that the gain of each scale varied by 1% between 0 and full scale—that is, that the gain of the amplifier was a sawtoothed function of intensity. This added sophistication increased the error of the mode-field diameter to 13 nm. I therefore took 13/$\sqrt{3}$ nm $\approx$ 8 nm to be the standard uncertainty that was due to gain nonlinearity.

H. Axial Position

The length of the arm is not significant, as long as the arm is longer than $100 \times w_0^2/\lambda$. Locating the fiber end at the center of rotation, however, is critical. If the length of the arm is L and the fiber end is located too close or too far from the detector by δL, then simple geometry shows that the relative error of the measurement is $\delta L/L$. If the fiber end lies in a plane

that is located within 25 μm of the axis, then the error of measurement is (25 μm)/(130 mm) times the true mode-field diameter or, in the case of the step-index fiber, approximately 2 nm. If we adopt this value as the 100% confidence interval, then the standard uncertainty is $2/\sqrt{3}$ nm ≈ 1 nm.

I. Cleave Angle

The cleaver we use normally produces an end that is perpendicular to the fiber axis within approximately 1 wavelength of visible light. This leads to an angle of approximately 4 mrad between the axis of the fiber and the axis of symmetry of the beam that emerges from the fiber. If the detector is to pass through the peak of the far-field radiation pattern, then the end of the fiber may have to be positioned nearly 0.5 mm from the center of rotation of the detector. One giant step is 0.4° or approximately 7 mrad and corresponds to a linear step of approximately 0.9 mm. Therefore, the angle of the endface, or cleave angle, may seem significant. It is possible to show, however, that the true angle between the fiber and the detector is equal to the nominal angle to second order in the position error. The main effect of the cleave angle is therefore to create a negligible cosine error.

Another effect of cleave angle is to put the fiber slightly farther from the detector than the nominal distance L because it lies in the correct plane but not on a radius of the circle. If the fiber is located a distance h from the center of rotation, then the extra distance δL is given by the sag formula $\delta L = h^2/2L$ and is less than 1 μm. The resulting error of the calculated mode-field diameter is less than 1 nm.

J. Vertical Position

In our system the fiber is positioned vertically with a micrometer while the photocurrent of the detector is maximized. For a step-index fiber whose mode-field diameter is approximately 9 μm, the vertical positioning is repeatable within approximately 100 μm. A vertical-positioning error results in a scan that does not follow a great circle of the reference sphere on which we are gathering data. Thus, whereas an error in the cleave angle as such may not be significant, an error in the positioning of the fiber may cause measurable error in the calculation.

If we were to scan across a small circle of the far-field pattern, rather than a great circle, then we might expect the measured mode-field diameter to be smaller than the true value. In the paraxial approximation, this is equivalent to scanning a chord rather than a diameter of the circ function. The length of that chord is less than the diameter by $h^2/2w$, where h is the vertical error and w is the radius of the circ function. We might therefore conclude that the measured mode-field diameter is larger than the true value by a few nanometers. This argument would be precisely correct if the far-field intensity pattern were a circ function.

If the near-field pattern is Gaussian, however, then the far-field pattern is nearly Gaussian. We restrict the discussion to the paraxial approximation. Suppose that the far-field pattern is given by the function $\exp(-R^2/w^2)$, where R is the distance from the center of the pattern. If we mistakenly scan a chord rather than a diameter, then we record $\exp[-(R^2 + h^2)/w^2]$, where h is again the vertical positioning error (out of the plane of Fig. 1). The near-field pattern is the Hankel transform of the far-field pattern and is equal to $\exp(-h^2/w^2) \times \exp(-r^2/w_0^2)$, that is, to a constant times the correct function. Therefore, in the Gaussian and paraxial approximations, the error that is due to a vertical offset is 0, not $h^2/2w$. As above, a rough but plausible approximation leads to error.

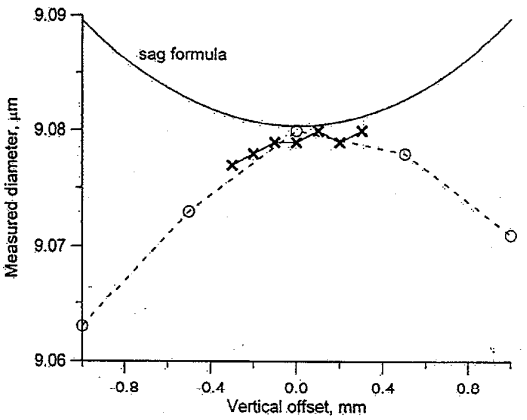

Fig. 5. Change of measured mode-field diameter as a function of vertical positioning error. The solid curve is an estimate based on the sag formula.

To directly assess the potential error caused by incorrect positioning, I measured the mode-field diameter of a step-index fiber as a function of vertical offset. The result is shown in Fig. 5. The crosses and open circles are different data sets made with the same fiber end. The mode-field diameter depends somewhat on vertical offset and, for this fiber, is slightly less than the value when the offset is 0 (not more, as predicted by the rough estimate). The sign of the uncertainty probably depends on the precise shape of the far-field pattern. For comparison, I show the rough estimate based on the sag formula.

If vertical positioning is accurate within 100 μm, then the 100% confidence interval is at most 2 nm, which I take to be the half-width of a symmetric interval because the uncertainty may differ for slightly different fibers. Thus the standard uncertainty is $2 \text{ nm}/\sqrt{3} \approx 1$ nm.

K. Lateral or Horizontal Position

If the fiber is offset laterally from the correct position, then, in the paraxial approximation, we detect the function $\exp[-2(R - h)^2/w^2]$, instead of the correct function, for which $h = 0$. The shift theorem of Fourier theory does not apply to the Hankel transform, because the derivation of the Hankel transform depends on the assumption of radial symmetry, and the shift from 0 to h breaks the symmetry. Depending on the sign of h, an integration from 0 to ∞ will yield

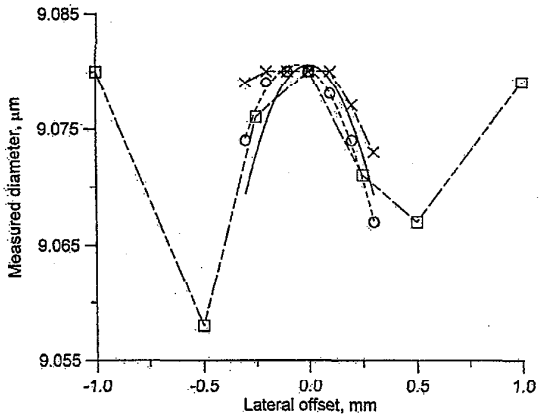

Fig. 6. Change of measured mode-field diameter as a function of lateral or horizontal positioning error. The open circles and squares are measured data. The dashed curve is a parabolic fit to the open-circle data. The solid curve is a theoretical curve that approximates the dashed curve. The crosses represent an attempt to correct for the offset mathematically.

a mode-field diameter that is, say, too small, whereas an integration from 0 to $-\infty$ will yield a result that is too large. The TIA solution is to average the two data sets and perform the integration once. Fiber-Optic Test Procedure 191 does not directly address the condition that the pattern is not precisely centered about 0.

We can rewrite the exponential function as $\exp[-2(R^2 - 2Rh + h^2)/w^2]$. The second-order term in h is a constant factor and does not contribute to the mode-field diameter. The first-order term, however, is significant, so the TIA's procedure does not completely correct for lateral errors. This is so because the sum of any two identical functions that display peaks near 0 but are offset from each other is necessarily broader than either function. Thus the function used for the calculation is necessarily broader than the true intensity pattern. The calculated mode-field diameter is therefore always less than the true value when there is a lateral offset in the position of the fiber.

To assess the error caused by a lateral offset, I aligned a fiber end as well as possible and then deliberately translated it laterally in successive 0.1-mm increments, performed a far-field scan, and calculated the mode-field diameter by averaging the two halves of the data set. The open circles in Fig. 6 show the results of such an experiment. A parabolic fit to the data (dashed curve) displays a maximum of 9.08 μm located −0.09 mm from the nominal center. This distance from the center is an estimate of the actual position of the fiber with respect to the center of rotation. It is approximately one tenth the distance traveled by the detector in a giant step of 0.4°.

I next added two Gaussian functions with a slight offset between them. The value of w_0 was set equal to 9.08 μm so as to agree with the parabolic fit. I integrated the sum according to Eq. (1). The result is shown as the solid curve in Fig. 6. Except for the offset, it parallels the dashed curved well.

I tried to correct for the offset by fitting a parabola to the first three data points, using that parabola to estimate the true center of the radiation pattern, and then carrying out the rest of the integration as before. The result is given by the crosses and the dot–dash curve. This formalism reduces the error by perhaps a factor of 3 but is not worth the effort because the error is small anyway. If, however, it is not practical to position the fiber accurately, this technique may reduce the required positioning accuracy measurably.

Finally, I repeated the experiment with offsets between −1 and +1 mm. These results are shown as the open squares in Fig. 6. The error introduced by a lateral offset is periodic, and the period is evidently determined by the offset that corresponds to the 0.4° giant step of the rotation stage. That is, as long as the fiber is directly opposite the detector at one position close to 0, the numerical calculation yields the correct result. The repeatability of locating the fiber is important, however, in that it must be well within 0.5 mm of the correct position to ensure an error less than 20 nm.

To estimate the uncertainty that results from lateral positioning errors, I assumed that the fiber could be positioned within 100 μm with approximately 100% confidence and that the probability could be evenly distributed over this interval (in reality, it is not). The resulting confidence interval is between 0 and −2 nm. Unlike the uncertainty owing to vertical offsets, this uncertainty is always negative. It is, however, so small that a correction is not necessary. As above, the standard uncertainty is 2 nm/$\sqrt{3} \approx 1$ nm.

L. Scattered Light

Scattered light adds to the far-field data a slowly varying function of angle, which we approximate as a constant. Adding this constant to the far-field intensity is the equivalent of adding a sombrero function to the near-field pattern (not convolving the near-field pattern with a sombrero function). Because the sombrero function adds more intensity where $\rho = 0$ than elsewhere, the near-field intensity is relatively sharply peaked near the center, and the calculated mode-field diameter is always less than the true value.

I assessed the effect of scattered light in two ways: First, I took the previous data sets and linearly added a constant. The smallest additive constant, 10^{-6}, is several times larger than my estimate of the scattered light in the system. The result is shown in Table 3 for both the step-index fiber and the dispersion-compensating fiber.

Scattered light has the most pronounced effect at the highest numerical aperture. This is so because the corresponding sombrero function in the near field is narrowest and therefore most sharply peaked at the highest numerical aperture. This result suggests that a scan should not be carried out farther

Table 3. Change of Mode-Field Diameter when a Constant Background is Added to Real Data

Angle (deg)	Background (relative units)	Step-Index Fiber (μm)	Dispersion-Compensating Fiber (μm)
21.2	0	9.081	
21.2	10^{-6}	9.079	
21.2	3×10^{-6}	9.074	
21.2	10^{-5}	9.057	
26	0	9.080	
26	10^{-6}	9.075	
26	3×10^{-6}	9.064	
26	10^{-5}	9.027	
40	10^{-5}	9.077	3.754
40	10^{-6}	9.052	3.754
40	3×10^{-6}	9.002	3.753
40	10^{-5}	8.834	3.750

than is necessary to reduce the error of truncating to less than a few nanometers if there is danger of scattered light entering the detector. When $\theta_m = 26°$, for example, the addition of a relative scattered intensity of 10^{-6} causes an error of −5 nm in the calculated mode-field diameter, whereas the same scattered intensity causes an error of nearly −30 nm when $\theta_m = 40°$.

Adding a constant to a real data set is problematic because those data already contain a measurable fraction of scattered light. The true value is therefore not necessarily the value calculated with the raw data. Accordingly, I performed a simulation using a Gaussian beam for the far-field pattern. The result is shown in Table 4. A relative scattered intensity of 10^{-6}, for example, causes an error of −4 nm when $\theta_m = 26°$ and −6 nm when $\theta_m = 28.8°$, which is in good agreement with the experiment. I therefore add a correction of 6 nm and adopt a standard uncertainty of $6/\sqrt{3}$ nm ≈ 3 nm.

M. Noncircularity of Fiber or Mode

The calculation, Eq. (1), assumes radial symmetry. The fiber core itself, however, may not be exactly circular, and the mode may not be circular even if the fiber is circular.

It is generally assumed that the mode is circular if the fiber is circular. The theory of the step-index fiber depends on the assumption that the z component E_z of the electric field is separable into the product of two functions, a function of radius and a function of azimuthal angle.[16] The lowest-order mode then has radial symmetry. It seems unlikely, however, that any mode can truly have radial symmetry (unless it is circularly polarized) because the boundary conditions where the electric field is parallel to the boundary and where it is perpendicular are different. In consequence, the phase shift on reflection for one linear component of polarization is different from that for the other component. Thus the mode is probably slightly oval, even in a perfectly circular fiber.

To estimate the order of magnitude of this effect, I calculated the TE and TM modes of a single-mode slab waveguide with parameters similar to those of the single-mode fiber. Specifically, the slab had a half-width of 4.33 μm, a cladding index of 1.457, and a core index of 1.4628. These parameters have no special significance except that they yielded a beam width of 9.087 μm for the TE mode and 9.073 μm for the TM mode, where here beam width means the full-width between the $1/e$ points. The mean value is 9.080 and is what we would expect with wholly unpolarized light. If the polarization were unknown, the uncertainty of a measurement (100% confidence interval) would therefore be approximately 7 nm, that is, the difference between 9.087 or 9.073 and their mean, 9.080.

The slab waveguide was meant as a model for a step-index fiber. Even a step-index fiber may have a slightly blurred interface, however. I examined a refracted-ray (refracted near field) scan[17] of another specimen of the same step-index fiber. Figure 7 shows two details from this scan. The points are 0.1 μm apart and are presented to facilitate an estimate of the edge transition widths. The leftmost scan is taken across the edge of the cladding. The 20–80% transition width is approximately 0.4 μm. Convolving the sombrero function with an edge shows that the 20–80% transition of a diffraction-limited system is equal to 0.63 times the theoretical resolution limit $0.61\lambda/\mathrm{NA}$, or approximately 0.38 μm. The system is therefore approximately diffraction limited.

The rightmost scan is the core of the fiber. The 20–80% transition width there is close to 0.8 μm, so we may assume that the core–cladding interface is slightly blurred or graded. The phase shift on reflection from a blurred or graded interface is $\pi/4$ and is independent of angle of incidence,[18] provided that the graded region is wide enough. Thus I interpret the 7-nm uncertainty implied by the slab waveguides as an upper limit to what we might expect in a real, circular fiber with a slightly graded interface.

The dispersion-compensating fiber has a small mode-field diameter and a correspondingly broad far-field intensity pattern. Far-field scans are therefore comparatively insensitive to lateral and vertical positioning errors. I made several scans of the dispersion-compensating fiber by placing a polarizer before the detector and adjusting the plane of the

Table 4. Change of Mode-Field Diameter when a Constant Background is Added to Simulated Data[a]

Background (relative units)	26°	28.8°
0	9.080	9.080
3×10^{-7}	9.079	9.078
10^{-6}	9.076	9.074
3×10^{-6}	9.066	9.060
10^{-5}	9.034	9.013

[a]Angular increment, 0.4°. Mode-field diameter is in micrometers.

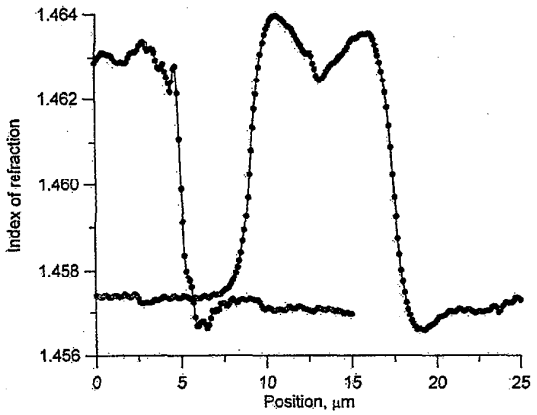

Fig. 7. Refractive-index profile of a step-index fiber. The left curve is the edge of the fiber and has a transition width of approximately 0.4 μm. The core displays a transition width of approximately 0.8 μm.

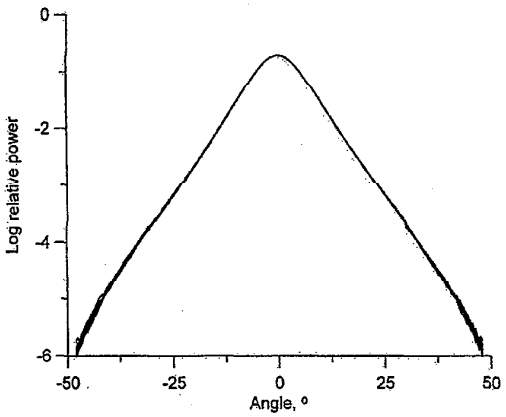

Fig. 8. Superposition of eight scans of a dispersion-compensating fiber with four orientations 90° apart and two orthogonal, linear polarizations at each orientation.

electric vector of the wave emerging from the fiber to be either horizontal or vertical, where vertical means perpendicular to the plane of the scan and horizontal means parallel to that plane. Without moving anything, I scanned the far field twice, once with each polarization, and divided the results point by point. I rotated the fiber approximately 90°, readjusted its position, and performed one more scan at each polarization. I repeated the procedure at angles of 180° and 270°.

Figure 8 superimposes all eight scans, and Fig. 9 superimposes the four ratios taken at each angle. The ratios are, within a few percent, equal to 1 out to an angle of 25°, where the intensity is a factor of 300 below the maximum. Integration from 0° to 25° contributes the majority of the final result. Nevertheless, the wave is not truly a TEM wave, and it might some day become necessary to account for that fact with fibers that have much smaller cores than most of today's fibers. The plots of Fig. 9 become noisy beyond 30°, where the denominators become small and noisy. It is not clear whether the apparent increase of the polarization ratio at large angles is real or the result of noise.

I performed similar experiments with the step-index fiber and calculated the mode-field diameters for vertical and horizontal polarizations. The horizontal polarization yielded a diameter that was on average 20 nm larger than the vertical, in fair agreement with the slab calculation, which yielded 14 nm.

The core of the fiber may be noncircular, and the fiber will therefore support a noncircular mode for this reason as well. It is impossible to distinguish noncircularity that is due to polarization from that due to noncircularity of the core without controlling the polarization.

Because the polarization in the fiber is in general unknown, the most probable value of the mode-field diameter is the average of the two linear polarizations. I took the 100% confidence interval that is due to polarization to be half the difference between horizontal and vertical polarizations, a half-width of approximately 10 nm. It is hard to distinguish, but the noncircularity of the fiber may add another ±10 nm, so I took the overall confidence interval that is due to the noncircularity of the mode to be $\sqrt{2} \times 10$ nm = 14 nm. The standard uncertainty is $14/\sqrt{3}$ nm ≈ 8 nm.

N. Wavelength

I measured the wavelength with a commercial grating instrument whose uncertainty is 0.1 nm, as measured at NIST. If the laser's wavelength is stable within another 0.1 nm, then the 100% confidence interval of the wavelength is 0.14 nm. The resulting confidence interval of mode-field diameter is (0.14 nm)/(1310 nm) times the mode-field diameter or, in our case, a bit less than 1 nm. The standard uncertainty is $1/\sqrt{3}$ nm ≈ 0.

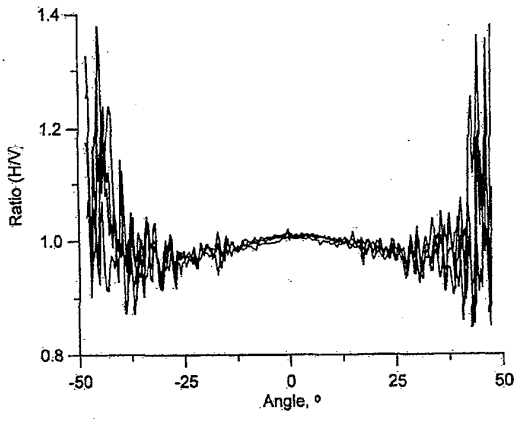

Fig. 9. Ratios of scans taken with orthogonal polarizations at each of the four orientations in Fig. 8.

Table 5. Summary of Uncertainties

Source	Method of Analysis	Correction (nm)	Uncertainty (nm)
Numerical integration	Simulation		<1
Angle of scan	Data	−5	3
Angular errors	Simulation plus specification		6
Finite pinhole	Simulation	8	2
Repeatability and noise	Data		3
Gain nonlinearity	Data plus simulation		8
Axial position of fiber	Geometry		1
Cleave angle	Geometry		<1
Vertical position	Data		<1
Lateral position	Data		1
Scattered light	Data plus simulation	6	3
Noncircularity	Measurements plus theory		8
Wavelength	Data		<1
Fresnel coefficients	Simulation plus theory		<1
Additive correction		9	
Combined uncertainty			15
Expanded uncertainty (coverage factor of 2)			30

O. Fresnel Coefficients

The Fresnel coefficients do not rigorously apply to the wave reflected from the end of the fiber. This is so for two reasons. First, they are derived for infinite plane waves incident on a semi-infinite medium. We can to some extent take this fact into account by decomposing the mode inside the cavity into its angular spectrum and calculating the amplitude transmittance for each component. The effect is slight; for example, for a Gaussian mode whose radius is 4.5 μm, the reflectance differs from the value at normal incidence by approximately 1 part in 10^6 at an angle of 5° and less than 2 parts in 10^5 at an angle of 10°. These angles correspond to 1 and 2 times the numerical aperture $\lambda/\pi w_0$ of the fiber. I nevertheless incorporated the Fresnel coefficients into the Gaussian simulation; they change the result of the calculation by less than 0.1 nm. I discuss the second reason in Subsection 4.R below.

P. Expanded Uncertainty

I calculated the expanded uncertainty for the step-index fiber only. Other similar fibers are probably subject to similar uncertainties, but fibers in different classes will need separate analyses. In addition, this analysis was carried out at 1310 μm. The mode-field diameter of the same fiber at 1550 μm is somewhat larger, but the uncertainties are largely unchanged.

The first column of Table 5 details all the uncertainties that I discovered, except for the effect of the reflection from the end of the fiber, and the second column describes the method of analysis. The third column shows the estimated corrections that are due to systematic errors or biased probability distributions. The last column shows the standard uncertainty, that is, with a coverage factor of $k = 1$. The second to last row shows the combined standard uncertainty, that is, the sum of the standard uncertainties added in quadrature. The last row shows the expanded uncertainty, that is, expanded to a coverage factor of 2 (which is analogous to 2 standard deviations of the mean).

Q. Philosophical Point 1

Before continuing, let us define the mode field and distinguish it from the aperture field. The mode field is the electric field inside the fiber but a great distance from either end, after evanescent waves have died away. If we call the exit face of the fiber the aperture plane, then the aperture field is the electric field in the aperture plane and differs from the mode field because different boundary conditions apply at the very end of the fiber. We may want to know the mode field for most applications, but we necessarily measure the aperture field.

Equation (1) has been derived from Petermann's definition of the mode-field radius:

$$w_0^{(P)} = \left[2 \int |e(r)|^2 r \, dr \Big/ \int |\partial e(r)/\partial r|^2 r \, dr \right]^{1/2}, \quad (4)$$

where $e(r)$ is the (scalar) mode field and the absolute value signs are for generality. (With the absolute value signs, we need not assume that $e(r)$ is real, that is, that the wave in the fiber is a TEM wave.) The integrations are carried out from 0 to ∞.

The derivation of Eq. (1) assumes both that the far-field pattern is equal to the Hankel transform of the near-field pattern and that the aperture field is the same as the mode field. Both assumptions are incorrect.

The far-field pattern is not equal to the Hankel transform but rather to the Hankel transform multiplied by a factor known as the obliquity or inclination factor.[19] That is,

$$E(\theta) = O(\theta)\mathrm{HT}[e_a(r)], \quad (5)$$

where HT stands for Hankel transform, $O(\theta)$ is the obliquity factor, and $e_a(r)$ is the aperture field. The obliquity factor is often ignored in calculations because it is nearly equal to 1 for small angles. In our calculation, however, angles are not necessarily small, and ignoring the obliquity factor selectively while otherwise using the exact theory is equivalent to commingling paraxial and exact calculations.

If we rewrite Eq. (5) as

$$E(\theta)/O(\theta) = \mathrm{HT}[e_a(r)] \tag{6}$$

and calculate the inverse Hankel transform

$$e_a(r) = \mathrm{HT}^{-1}[E(\theta)/O(\theta)], \tag{7}$$

we find that the Hankel transform pair consists of $e_a(r)$ and $E(\theta)/O(\theta)$, not $e_a(r)$ and $E(\theta)$. The function $I(\theta)$ in Eq. (1) should therefore be replaced with $I(\theta)/O^2(\theta)$, because $I(\theta) = |E|^2(\theta)$ in the far field.

We argued earlier that the obliquity factor in scalar theory is equal to $\cos\theta$,[20,21] not $(1 + \cos\theta)/2$. If we adopt Petermann's definition, Eq. (3), but include the obliquity factor, we find

$$2w_0^{(\mathrm{P}')} = (\lambda/\pi)\left[2\int I(\theta)\tan\theta\,\mathrm{d}\theta \Big/ \int I(\theta)\sin^2\theta\tan\theta\,\mathrm{d}\theta\right]^{1/2}. \tag{8}$$

Equation (8) follows rigorously from applying Petermann's definition to the aperture field and could therefore be considered the correct result for scalar theory.

To assess the effect of using Eq. (8) in place of Eq. (1), I first performed a simulation using a Gaussian beam and an angular scan with $\theta_m = 26°$. Including the obliquity factor in the calculation decreased the mode-field diameter by approximately 20 nm. With the real, step-index fiber, the decrease was more nearly 25 nm. With the dispersion-compensating fiber, the decrease grew from 80 to 100 nm as θ_m increased from 26° to 40°. That is, including the obliquity factor in the calculation may change the result by as much as 100 nm with a particularly small-cored fiber, but perhaps −25 nm with a common step-index fiber.

The difference between the two calculations, including or not including the obliquity factor, is not an uncertainty. To the contrary, if the calculation that includes the obliquity factor is correct—or more nearly correct than the simpler theory—then the simpler calculation gives rise to a systematic error.

Both Eqs. (1) and (8) may be transformed to the near field by applying standard Fourier transform theorems. Both are derived, with different assumptions, from Petermann's original definition, Eq. (3). Equation (3) pertains to the mode field of a fiber, not the aperture field. Truncating the fiber, however, excites fields that are radiative and decay asymptotically as $1/r$ in the far field. The numerator and denominator of Eq. (3) therefore diverge: In general, $w_0^{(\mathrm{P}')}$ does not exist.

The mode-field radius $w_0^{(\mathrm{P}')}$ as defined by Eq. (8) likewise does not exist. The definition as stated in Eq. (1), by contrast, converges but does not correctly follow from Petermann's definition, Eq. (3), as applied to the aperture field. We therefore suggested elsewhere that Eq. (1), though arguably incorrect, be adopted as the definition of mode-field diameter.[22] This has an advantage in that it is consistent with present practice.

Let the field a short distance z beyond the aperture plane be $e_a(r, z)$, where $z = 0$ is the plane of the face and $e_a(r) = e_a(r, 0)$. In terms of the field in the plane defined by z, the far-field pattern can be expressed as

$$E(\theta) = O(\theta)\mathrm{HT}[e_a(r, z)]\exp(ik_z z), \tag{9}$$

where $O(\theta) = \cos\theta$ and $k_z = k\cos\theta$ is the z component of the propagation vector. Inverting Eq. (9), we find

$$e_a(r, z) = \mathrm{HT}^{-1}[E(\theta)/O(\theta)]\exp(-ik_z z). \tag{10}$$

Taking the derivative of both sides of Eq. (10) with respect to z brings out a factor of $\cos\theta$, which cancels the divisor $O(\theta)$. Apart from a constant factor, $\partial e_a(r, z)/\delta z$ and $E(\theta)$ are a Hankel transform pair, whereas $e_a(r, z)$ and $E(\theta)$ are not. This consideration leads to the alternative near-field expression

$$w_0^{(a)} = \left[2\int |e_a'(r)|^2\, r\mathrm{d}r \Big/ \int |\partial e_a'(r)/\partial r|^2 r\mathrm{d}r\right]^{1/2}, \tag{11}$$

where $e_a'(r) = [\partial e_a(r, z)/\partial z]_{z=0}$. If we calculate the far-field relation that corresponds to Eq. (11), we derive Eq. (1); that is, $w_0^{(a)} = w_0$. This result suggests that we adopt Eq. (11) in place of Eq. (3) as the near-field expression for w_0. In the region near the core, the aperture field is very nearly a TEM wave (and is probably very nearly equal to the mode field), so Eq. (11) reduces to Petermann's original definition, Eq. (3). Equation (9) converges, however, whereas Eq. (3) will not converge if $e(r)$ is replaced by the aperture field $e_a(r)$. Applying Eq. (9) experimentally to near-field scans, unfortunately, may be difficult in cases in which the aperture field is not very nearly a TEM wave because the near-field scan measures intensity, not the axial derivative of the field. Thus we should expect small discrepancies between near- and far-field measurements of w_0.

R. Philosophical Point 2

The wave at the end of the fiber experiences a discontinuity in index of refraction. It is for this reason that the aperture field differs from the mode field. We may well want to know the mode field, however, not the aperture field, as when two fibers are connected end to end. If the fibers are aligned fairly well, the field at their intersection probably closely approximates the mode field, rather than the aperture field at the end of a truncated fiber.

We can estimate the effect of truncating the fiber by simply assuming that the field just outside the

fiber is equal to the field just inside times the transmittance given by the Fresnel coefficient. That is, we assume that the transmittance of the part of the wave inside the core is slightly different from the transmittance of the part of the wave in the cladding. This approximation is precisely the approximation that Kirchhoff made in his analysis of diffraction by an aperture in an opaque screen and is sometimes called the Kirchhoff approximation. It ignores both evanescent and propagating waves created as the result of the discontinuity.

Let us assume that the beam inside the fiber is Gaussian and has radius w_0. The fiber core has radius a and index of refraction $n_0 = 1.4572$, and the cladding has index $n_1 = 1.4630$. The corresponding amplitude reflectances r_0 and r_1 differ by approximately 0.002 at normal incidence. Applying the Kirchhoff approximation, we can write the electric field just outside the fiber as

$$e(r) = \exp(-r^2/w_0^2)[1 - (r_1 - r_0)\mathrm{circ}(r/a)], \quad (12)$$

where $\mathrm{circ}(r/a) = 1$ when $r < a$ and 0 otherwise. The far-field pattern is then

$$E(\sin\theta)/O(\theta) = \exp(-\sin^2\theta/\sin^2\theta_0) - (r_1 - r_0) \times \exp(-\sin^2\theta/\sin^2\theta_0)*\mathrm{somb}(a\xi), \quad (13)$$

where the sombrero function has been defined in Subsection 4.C., * means convolution, and $\mathrm{somb}(a\xi)$ is the Hankel transform of $\mathrm{circ}(r/a)$. The far-field intensity is

$$I(\theta)/O^2(\theta) = \exp(-2\sin^2\theta/\sin^2\theta_0) - 2(r_1 - r_0)\exp(-\sin^2\theta/\sin^2\theta_0) \times [\exp(-\sin^2\theta/\sin^2\theta_0)*\mathrm{somb}(a\xi)], \quad (14)$$

where the term that contains $(r_1 - r_0)^2$ is neglected.

The second term on the right of Eq. (14) is the result of the difference between the mode field and the aperture field. The core radius a of the step-index fiber is approximately 4.2 μm, so the first zero of the sombrero function lies where $\sin\theta = 0.61\lambda/a$, or where $\theta = 11°$. The mode-field radius w_0 is 4.5 μm, so $\theta_0 = 5.3°$. Thus the second term in Eq. (14) is somewhat broader than the first and is therefore significant at all angles. Because $2(r_1 - r_0)$ is approximately 0.004, this term may be significant. It does not represent an error but rather is part of the far-field diffraction pattern. That is, the difference between the mode of the fiber and the aperture field may appear in the measured far-field pattern. For connector studies, there is no fiber–air interface, so the mode field may be what is important. In the future it may become necessary to distinguish between the aperture field and the mode field.

I thank Ron Wittmann of the NIST Electromagnetic Fields Division for endlessly rereading this paper and developing the mathematics related to Subsection 4.Q. Andy Hallam of PK Technology initiated discussions about the obliquity factor and also made incisive comments on the paper. Jerry Benson and Brian Walker of the National Physical Laboratory (UK) and Arthur Barlow of EG&G likewise read and commented on the paper. Thanks also to Silvia Mioc for providing her data, which are displayed in Fig. 3; to Norm Fontaine for measuring the index profile of the step-index fiber and supplying Fig. 7; and to Igor Vayshenker for providing the calibrated spectrum analyzer. Finally, Jack Wang and Barry Taylor of NIST helped with the uncertainty analysis, Brad Alpert of NIST helped with the numerical integration, and Doug Matovich of Aerotech patiently explained the systematic errors in a rotation stage. Contribution of the National Institute of Standards and Technology, not subject to copyright.

References

1. Anonymous, "Measurement of mode field diameter of single-mode optical fiber," Fiberoptic Test Procedure FOTP-191, Telecommunications Industry Association, 2500 Wilson Blvd., Suite 300, Arlington, Va. 22201-3834 (1998).
2. K. Petermann, "Constraints for fundamental-mode spot size for broadband dispersion-compensated single-mode fibres," Electron. Lett. **19,** 712–714 (1983); C. Pask, "Physical interpretation of Petermann's strange spot size for single-mode fibres," Electron. Lett. **20,** 144–145 (1984).
3. M. Artiglia, G. Coppa, P. Di Vita, M. Potenza, and A. Sharma, "Mode field diameter measurements in single-mode optical fibers," J. Lightwave Technol. **7,** 1139–1152 (1989).
4. D. L. Franzen, M. Young, A. H. Cherin, E. D. Head, M. J. Hackert, K. W. Raine, and J. G. N. Baines, "Numerical aperture of multimode fibers by several methods: resolving differences," J. Lightwave Technol. **7,** 896–900 (1989); E. M. Kim and D. L. Franzen, "Measurement of far-field radiation patterns from optical fibers," in *Optical Fiber Characterization*, G. E. Chamberlain, G. W. Day, D. L. Franzen, E. M. Kim, and M. Young, eds. Natl. Bur. Stand. (U.S.) Spec. Publ. 637 (U.S. GPO, Washington, D.C., 1983), Vol. 2, Chap. 4.
5. M. Young, *Optics and Lasers, including Fibers and Optical Waveguides*, 4th ed. (Springer, New York, 1993), Sec. 5.5.4; see also M. Young, "The pinhole camera," Phys. Teacher **27,** 648–655 (1989); "Pinhole optics," Appl. Opt. **10,** 2763–2767 (1971).
6. M. Young, *Optics and Lasers, including Fibers and Optical Waveguides*, 4th ed. (Springer, New York, 1993), Chap. 4, especially Eqs. (4.2), (4.3), and (4.22).
7. M. Young, "Can you describe optical surface quality with one or two numbers?" in *Optical Specifications: Components and Systems*, W. J. Smith and R. E. Fischer, eds., Proc. SPIE **406,** 12–22 (1983).
8. T. J. Drapela, D. L. Franzen, A. H. Cherin, and R. J. Smith, "A comparison of far-field methods for determining mode field diameter of single-mode fibers using both Gaussian and Petermann definitions," J. Lightwave Technol. **7,** 1153–1157 (1989).
9. Anonymous, *Guide to the Expression of Uncertainty in Measurement* (International Organization for Standardization, Case postale 56, CH-1211, Genève 20, Switzerland, 1993).
10. J. W. Gaskill, *Linear Systems, Fourier Transforms, and Optics* (Wiley, New York, 1978), pp. 266–272.
11. P. S. Lovely and C. S. Shaar, "Systematic errors in measurement of mode field diameter," in *Fiber Optic Networks & Coherent Technology in Fiber Optic Systems II*, J. D. Chipman and H. R. D. Sunak, eds., Proc. SPIE **841,** 240–247 (1987).
12. W. H. Press, B. P. Flannery, S. A. Teukolsky, and W. T. Vet-

tering, *Numerical Recipes in C* (Cambridge U. Press, New York, 1992), Chap. 4.
13. Ref. 10, Chap. 3.
14. W. T. Anderson, V. Shah, L. Curtis, A. J. Johnson, and J. P. Kilmer, "Mode-field diameter measurements for single-mode fibers with non-Gaussian field profiles," J. Lightwave Technol. **LT-5**, 211–217 (1987).
15. K. Enslein, A. Ralston, and H. S. Wilf, *Statistical Methods for Digital Computer* (Wiley, New York, 1977).
16. A. H. Cherin, *An Introduction to Optical Fibers* (McGraw-Hill, New York, 1983), Sect. 5-2.
17. M. Young, "Optical fiber index profiles by the refracted-ray method," Appl. Opt. **20**, 3415–3422 (1981).
18. A. B. Sharma, S. J. Halme, and M. M. Butusov, *Optical Fiber Systems and Their Components* (Springer, New York, 1981), Sec. 3.4.
19. J. W. Goodman, *Introduction to Fourier Optics* (McGraw-Hill, San Francisco, Calif., 1968); M. Born and E. Wolf, *Principles of Optics* (Pergamon, Oxford, 1980).
20. M. Young and R. C. Wittmann, "Vector theory of diffraction by a single-mode fiber: application to mode-field diameter measurements," Opt. Lett. **18**, 1715–1717 (1993).
21. A. Sommerfeld, *Optics: Lectures on Theoretical Physics* (Academic, New York, 1964), Vol. 4, Sec. 34.
22. R. C. Wittmann and M. Young, "Are the formulas for mode-field diameter correct?," submitted to the Symposium on Optical Fiber Measurements, Boulder, Colo., 15–17 September 1998.